

Does the subtropical jet catalyze the mid-latitude atmospheric regimes?

PAOLO M. RUTI⁽¹⁾, VALERIO LUCARINI⁽²⁾, ALESSANDRO DELL' AQUILA⁽¹⁾, SANDRO CALMANTI⁽¹⁾, ANTONIO SPERANZA⁽²⁾,

¹*Progetto Speciale Clima Globale, Ente Nazionale per le Nuove Tecnologie, l'Energia e l'Ambiente, Roma, Italy*

²*Dipartimento di Matematica ed Informatica, Università di Camerino, Camerino (MC), Italy*

Abstract

Understanding the low-frequency variability of the atmosphere, is of crucial importance in fields such as climate studies, climate change detection, and extended-range weather forecast. The Northern Hemisphere climate features the planetary waves as a relevant ingredient of the atmospheric variability. Several observations and theoretical arguments seem to support the idea that indicators of the winter planetary waves activity obey a non-gaussian statistics and may present a multimodal probability density function, characterizing the low-frequency portion of the climate system. We show that the upper tropospheric jet strength is a critical parameter in determining whether the planetary waves indicator exhibits a uni- or bimodal behavior, and we find out the relevant threshold value of the wind speed. These results are obtained considering the overlapping period of the NCEP-NCAR and ECMWF reanalyses (1958-2002). Our results agree with the physical framework proposing the nonlinear wave self-interaction as the basic mechanism

establishing the statistical non-normality of the low-frequency variability of the atmosphere and its possible bimodality.

The notion that well-defined winter mid-latitude atmospheric “patterns of flow” are “recurrent” during the northern hemispheric winters¹ has been repeatedly put forward, investigated and debated since the early definition of Grosswetterlage², to the classical identification of Atlantic blocking³, all the way to more recent work on regime detection and identification⁴. When set in a rigorous statistical framework, the identification of regimes requires their clustering in an appropriate parameter space, although the clustering operation may be controversial⁵. Once identified, one clustering maximum of probability may result associated either to persistency or to frequent visitation of the surroundings of the maximum probability configuration, or any combination thereof. A classical physical model for the first type of behaviour is the potential well with stochastic noise. This type of model, albeit basically heuristic in the research context proposed here, can considerably help in assessing the statistical properties and identifying the dominant physical processes of very complex systems. In such a perspective, the relevant problem concerning the general circulation of the atmosphere has been understanding whether the large scale atmospheric circulation undergoes fluctuations around a single equilibrium⁵ or if it continuously switches among multiple equilibria^{4,6-13}. The understanding of this climatic property responds to practical needs such as the feasibility of extended range weather forecasts or the robust detection of climate changes⁴.

Coming to the dominant physical processes, the mid-latitude dynamics feature upper tropospheric westerlies and synoptic to planetary waves as typical ingredients. The radiative forcing and the Earth rotation constrain the

characteristics of the mean axially symmetric circulation and thereby the strength of the midlatitude westerly winds (jet)¹⁴. A theory was required to account for the observed multimodal (or, anyway, non-normal) distribution of an indicator of the activity of planetary waves^{7,16}, which constitute the low frequency component of the atmospheric variability. The planetary waves were soon assumed to be related to orographic resonance processes⁶. At first, the wind-wave interaction was proposed as driving mechanisms allowing for the establishment of multiple equilibria of the planetary waves amplitude⁶. However, the transitions between the quasi-stable equilibria require for energetic reasons large variations ($\Delta u \approx 40 m s^{-1}$) of the mean westerlies, at odds with the “normality” of the distribution of the observed westerlies strength ($u \approx 30 m s^{-1}$)^{16,17}. Therefore, a dynamical interpretation featuring fixed strength of the westerlies was required. The bent resonance curve obtained in non-linear wave self interaction theories¹⁷ (Figure 1), not only explains the existence of the multiple equilibria of the planetary wave amplitude⁷, but also includes the possibility that relatively small changes of the jet strength may imply a switch from unimodal to multimodal regimes of the atmospheric circulation.

In this study, we take advantage of a longer observational basis, consisting of the two major reanalysis products released by NCEP-NCAR and by ECMWF (hereafter NCEP and ERA40, respectively), which span the period from 1958 to 2002^{18,19}. The discrepancies of the two re-analyses have been previously analyzed in the spectral domain²⁰. The proper counterparts to the dynamical parameters employed in the theories are extracted from such datasets by computing two robust indicators of the state of relevant large scale features of the mid-latitude troposphere. The Wave Activity Index⁷ (WAI) is computed as the root mean

square of the zonal wavenumbers 2 to 4 of the winter 500 hPa geopotential height variance over the channel 32°N – 72°N. Such an index is aimed at providing a synthetic picture of the ultra long planetary waves and at capturing the orographic resonance, since an approximate mode of zero phase velocity (resonance) is 3¹⁶. The Jet Strength Index (JSI) is computed as the daily maximum of the zonal mean of the zonal wind at 200hPa, which always peaks between 30°N and 35°N.

We first assess the overall equivalence of the picture provided by the winter WAI and JSI extracted from the two reanalyses, by performing one-dimensional and two-dimensional Kolmogorov-Smirnov test^{21,22} on the distribution of the single variables and on the joint pdfs. In both cases, the pdfs are equivalent at a confidence level larger than 95%. Therefore, we can safely consider the results obtained with NCEP as representative for both reanalyses and highlight the main differences where necessary.

The empirical joint pdf, constructed by means of two-dimensional gaussian estimators (Figure 2) presents multiple, well defined, peaks distributed over the WAI-JSI space. A major peak (point A in Figure 2) corresponds to weak upper tropospheric jet (JSI ~ 40 m s⁻¹) and low to intermediate activity of the planetary waves (WAI ~ 60 m). Two other peaks (points B and C) correspond to intermediate strength of the jet and to well-separated (~ 15 m) values of the WAI. A fourth minor peak (point D) corresponds to very strong jets and relatively low level of planetary wave activity.

These features are qualitatively reproduced in the picture sketched in Figure 1, where three different regions can be separated, characterized by low, intermediate and high intensities of the tropospheric jet and by a different number of equilibrium amplitudes of the planetary waves.

While the 2d joint pdf has essentially the role of providing a qualitative view on the properties of the system, a more stringent statistical interpretation of such analogy can be highlighted by considering the distribution of WAI obtained by fixing the range of JSI variability. Guided by the conceptual framework of the bent resonance and given the location of the peaks of the joint WAI-JSI distribution, we split the entire WAI-JSI space into three sectors, characterized by low ($38 \text{ m s}^{-1} < \text{JSI} < 41 \text{ m s}^{-1}$), intermediate ($42 \text{ m s}^{-1} < \text{JSI} < 47 \text{ m s}^{-1}$) and high ($48 \text{ m s}^{-1} < \text{JSI} < 52 \text{ m s}^{-1}$) intensities of the jet, each sector comprising about 1/6, 1/3, and 1/6 of the total sample population, respectively.

The empirical distributions of WAI (Figure 2 b) are meant to be a statistically robust representation of the atmospheric planetary waves in each subrange of the JSI values. Well-distinct peaks are observed in the intermediate range, while for weak or strong JSI unimodal distributions appear. Strong oceanic tropical forcing (El Nino)²³ implies zonal elongation and strengthening of the sub-tropical jet respect to normal conditions, resulting in strong JSI (more than 48 m/s), and locating the El Nino years in the upper region of the phase-space (Figure 2a).

Statistical robustness in the properties of the pdfs is required in order to avoid artificial results⁵. Since we are testing the hypothesis of having a specific number of peaks in each of the considered JSI sub-range, we estimate the optimal kernel width h by generating an ensemble of surrogate datasets (1000 members) and then choosing the value of h that maximizes the trade-off between having as many surrogate distributions with the correct number of peaks and as few surrogate distributions with the wrong number of peaks. The surrogate datasets are generated with a bootstrap Montecarlo experiment in which 45 winters are selected randomly with repetition among the reanalysis period lasting from 1958

to 2002. After spanning systematically a whole range of values of h we find that the best trade-off is realized for $h = 3.5 \text{ m}$, in close agreement with a recent study²⁴.

The values reported in table 1 show, e.g., that the hypothesis that the bimodal distribution for intermediate values of JSI occurs by chance can be rejected with a good level of statistical confidence (higher for NCEP than for ERA40).

We have that, for such a value of the smoothing parameter, the position and height of the peaks of wave activity corresponding to each class of intensity of the upper tropospheric jet are safely characterized in a statistical sense. In particular, the two peaks observed for intermediate values of JSI are well separated ($\sim 15 \text{ m}$). Moreover, the two reanalyses agree in the position of the peaks, despite the different degree of statistical confidence. These properties allow for a diagnostic characterization of the corresponding flow regimes. Our results appear robust since similar and consistent results – although with different degree of statistical confidence – are obtained with all the values of h ranging from 2 m to 5 m.

Using the density pdfs given in Figure 2b to stratify the data, mean maps for all days corresponding to the peaks of the bimodal distribution and of the unimodal distributions have been computed (see the caption for the details of the computation). The difference map between the two intermediate JSI patterns B and C indicates a more amplified wave number three component for the pattern C, with higher geopotential height centers over the northern Pacific and Alaska, the Northern Sea, and the Siberian land. The wavenumber three appears to be the most resonant in the Northern Hemisphere. The eddy field corresponding to the low JSI (pattern A) shows the lowest ridge over the Rockies and the higher

Greenland through, with respect to the pattern B and pattern C. Finally, the eddy field for the high JSI (pattern D) shows the highest ridge over the Rockies.

Overall, our analysis indicates that in the Northern Hemisphere the statistics of the planetary atmospheric waves can be characterized in terms of the sub-tropical jet, consistently with the physical framework proposing the nonlinear modification of the topographic resonance due to the nonlinear wave self-interaction¹⁷ as the basic mechanism for the low-frequency variability of the atmosphere. We have proved on the available NCEP and ERA 40 global reanalyses that for intermediate jet strength, an indicator of the planetary waves presents a bimodal behavior, while for higher or lower values of the jet strength the estimated pdf is unimodal. Thus, the interpretation of the interaction between the tropics and the mid-latitudes should be addressed not only considering the wave trains emanating from the tropics²⁵, but also in the perspective of the role of the sub-tropical jet in defining the statistical properties of the planetary waves. The zonal mean circulation (Hadley circulation), and the tropical oceanic forcings (i.e. ENSO), play a relevant role in this view. In this perspective, the strongest El Nino years could be located in the upper branch of a hysteresis cycle, where the system undergoes a unique solution.

Finally, we note that these results entail the requirement for models, used to perform scenario for the Fourth Assessment Report of the IPCC (IPCC-4AR) or to produce seasonal forecasts, to accurately simulate the nonlinear ultralong wave self-interactions in order to capture the main features of the low frequency variability of the atmosphere. This topic is addressed in a subproject of the Program for Climate Model Diagnosis and Intercomparison (PCMDI), which is

expected to provide a scientific basis for the IPCC-4AR.

Methods.

Data.

In this work, we consider the winter-time daily fields of the 500 hPa geopotential height and of the 200 hPa zonal wind, for the overlapping time frame ranging from December 1st 1957 to August 31st 2002. We use the data from two reanalyzed datasets, provided by the National Center for Environmental Prediction (NCEP), in collaboration with the National Center for Atmospheric Research (NCAR)¹⁸ and by the European Center for Mid-Range Weather Forecast (ECMWF)¹⁹. Both reanalyses are publicly released with a horizontal spatial resolution of 2.5° x 2.5° on each pressure level, resulting into a horizontal grid of 144 x 73 points.

Computation of the planetary wave index.

Following previous works^{7,15} we average the daily 500hPa geopotential field over a latitudinal belt. We identify an objective criteria as follows. For each day in the DJF period, 500 hPa geopotential height is Fourier decomposed in the longitudinal direction, λ ; the amplitude of the index is obtained from the variance associated to the Fourier coefficients of the zonal wavenumbers $k=2-4$ (see formula below) as a function of the latitude. The variance of the index is computed as a function of the latitude and using the half height criteria the minimum and maximum latitude are selected (32°N-72°N). We then compute for each day the discrete spatial Fourier transform of the field, and define the so called wave activity index (WAI) as follows:

$$(1) \quad WAI(t) = \left(\sum_{k=2}^k 2 \cdot |A_k(t)|^2 \right)^{1/2},$$

where $|A_k(t)|$ is the Fourier coefficient of the wave having wavenumber k at the time t .

Index time filtering.

WAI. In order to attenuate the direct influence of the seasonal cycle we erase from the signal its first 4 harmonics of the $1y^{-1}$ frequency. Along the same lines, in order to mitigate the signature of the synoptic atmospheric variability, we apply a low-pass filter by performing a 5-day running mean to the signal.

JSI. In order to mitigate the signature of the synoptic atmospheric variability, we then apply a low-pass filter by performing a 5-day running mean to the signal. Since in the context of the bent resonance theory¹⁷ the jet strength is considered as an autonomous forcing parameter of the system, we do not filter out from the JSI the seasonal cycle and its harmonics as done for the WAI. Obviously, within a linear reasoning, the cancellation of these frequencies performed on the WAI hides part of the influence of the jet strength, but we assume that such effect is noticeably smaller than the direct influence of the seasonal cycle itself.

Kolmogorov-Smirnov test.

The Kolmogorov-Smirnov test (K-S-test) tries to determine whether one-dimensional data sample is compatible with being a random sampling from a given distribution. It is also used to test whether two data samples are compatible with being random samplings of the same, unknown distribution. The K-S test is only appropriate for testing data against a continuous distribution and has the advantage of making no assumption about the distribution of data.

Kernel density estimator²⁶.

The goal of n-dimensional density estimation is to approximate the joint pdf $f(x_1, \dots, x_n)$ of n-dimensional random variables (X_1, \dots, X_n) . Assume we have N observations $(x_{1,k}, \dots, x_{n,k})$ $k = 1..N$ for the random variables. The kernel density estimator $\hat{f}_{h_1, \dots, h_n}(x_1, \dots, x_n)$ can be written as:

$$\hat{f}_h(x) = \frac{1}{N h_1 \dots h_n} \sum_{k=1}^N K\left(\frac{x_1 - x_{1,k}}{h}, \dots, \frac{x_n - x_{n,k}}{h}\right),$$

where $K(x_1, \dots, x_n)$ is the Kernel function and (h_1, \dots, h_n) is the vector of the smoothing parameters. Various functional forms for $K(x)$ are widely used in the literature; we have adopted the conventional Gaussian form. For our 2D case, we then have $K(x_1, x_2) = 1/2\pi \cdot \exp(-1/2 x_1^2 - 1/2 x_2^2)$, while for the 1D case we have $K(x) = 1/\sqrt{2\pi} \exp(-1/2 x^2)$. With this choice the empirical pdfs are normalized to 1.

Composites of the patterns

In order to characterize the patterns B and C revealed for intermediate values of JSI, we composite the days when WAI is bounded in the interval with the centre on the local pdf maximum and the range corresponding to the double distance between the considered maximum and the intermediate dip value. To illustrate the most populated mode for low and high JSI (pattern A and D) we consider the amplitude range of WAI corresponding to the half height of the distribution.

References

1. Dole, R. M., Persistent anomalies of the extratropical Northern Hemisphere wintertime circulation. *Large-Scale Dynamical Processes in the Atmosphere*, B. J. Hoskins and R. P. Pearce, eds., Academic Press, NY, 95-109 (1983).
2. Baur, F. Extended range weather forecasting. *Compendium of Meteorology*, Amer. Meteorol. Soc., 814-833 (1951).
3. Rex, D.F. Blocking action in the middle troposphere and its effect upon regional climate. Part 2: The climatology of blocking action. *Tellus*, **2**, 275-301 (1950).
4. Corti, S., Molteni F., Palmer, T.N. Signature of recent climate change in frequencies of natural atmospheric circulation regimes. *Nature*, **398**, 799-802 (1999).
5. Stephenson, D.B., Hannachi, A., O'Neill, A. On the existence of multiple climate regimes. *Quart. J. Roy. Met. Soc.*, **130**, 583-605 (2004).
6. Charney, J. G., Devore, J.C. Multiple flow equilibria in the atmosphere and blocking. *J. Atmos. Sci.*, **36**, 1205-1216 (1979)
7. Hansen, A.R., Sutera, A. On the probability density distribution of Planetary-Scale Atmospheric Wave amplitude. *J. Atmos. Sc.*, **24**, 3250-3265 (1986).
8. Mo, K., Ghil, M. Cluster analysis of multiple planetary flow regimes. *J. Geophys. Res.*, **93**, 10927-10952 (1988).
9. Molteni, F., Tibaldi, S., Palmer, T.N. Regimes in the wintertime circulation over northern extratropics. I: Observational evidence. *Quart. J. Roy. Met. Soc.*, **116**, 31-67 (1990).
10. Vautard, R., Multiple weather regimes over the North Atlantic. Analysis of precursors and successors. *Mon. Wea. Rev.*, **118**, 2056-2077, (1990).
11. Cheng, X., Wallace, J.M. Cluster analysis of the Northern Hemisphere winter-time 500 hPa height field: spatial patterns. *J. Atmos. Sci.*, **50**, 2674- 2696 (1993).
12. Kimoto, M., Ghil, M. Multiple flow regimes in the Northern Hemisphere winter, part I: methodology and hemispheric regimes. *J. Atmos. Sci.*, **50**, 2625-2643 (1993).
13. Hannachi, A., Legras, B. Simulated annealing and weather regimes classification. *Tellus*, **47**, 955-973 (1995).
14. Held, I.M, Hou, A.Y. Nonlinear axially symmetric circulations in a nearly inviscid atmosphere. *J. Atmos. Sc.*, **37**, 515-533 (1981).
15. Benzi, R., Speranza, A., Statistical properties of low frequency variability in the Northern Hemisphere. *J. Climate* **2**, 367-379 (1989).
16. Malguzzi, P., Speranza, A. Local Multiple Equilibria and Regional Atmospheric Blocking. *J. Atmos. Sc.*, **9**, pp. 1939-1948 (1981).
17. Benzi R., Malguzzi, P., Speranza, A., Sutera, A. The statistical properties of general atmospheric circulation: observational evidence and a minimal theory of bimodality. *Quart. J. Roy. Met. Soc.*, **112**, 661-674 (1989).
18. Kistler R, et al. The NCEP-NCAR 50-year reanalysis: Monthly means CD-ROM and documentation. *Bull. Am. Meteorol. Soc.* **82**, 247-267 (2001)
19. Simmons, A. J., Gibson, J.K. The ERA-40 Project Plan, ERA-40 Project Report Series No. 1, ECMWF, 62 pp (2000).
20. Dell'Aquila, A., Lucarini, V., Ruti, P.M., Calmanti, S. Hayashi Spectra of the Northern Hemisphere Mid-latitude Atmospheric Variability in the NCEP-NCAR and ECMWF Reanalyses. *Accepted by Climate Dynamics* (2005).
21. Peacock, J.A. Two-dimensional goodness-of-fit testing in astronomy. *Mon. Not. R. Astr. Soc.* **202**, 615-627 (1983).
22. Fasano, G., Franceschini, A. A multidimensional version of the Kolmogorov-Smirnov test. *Mon. Not. R. Astr. Soc.* **225**, 155-170 (1987).
23. Philander, S.G. *El Nino, La Nina, and the Southern Oscillation*. San Diego - Academic Press (1990)
24. Christiansen, Bo, On the bimodality of planetary-scale atmospheric wave amplitude index. *J. of Climate*. In press (2005).
25. Hoskins, B.J., Ambrizzi, T. Rossby wave propagation on a realistic longitudinally varying flow. *J. Atmos. Sc.*, **50**, 1661-1671 (1993).
26. Silverman, B.W. *Density Estimation for Statistics and Data Analysis*. Chapman & Hall (1986).

End Notes.

Acknowledgments. The authors wish to thank A. Sutera for useful suggestions. NCEP data have been provided by the NOAA-CIRES Climate Diagnostics Center, Boulder, Colorado, from their web site at <http://www.cdc.noaa.gov/>. The ECMWF ERA-40 data have been obtained from the ECMWF data server at <http://data.ecmwf.int/data/>.

Author Contributions. This work is based on a s-meeting held at the University of Camerino in July 2004. A s-meeting means few days workshop focused on 2-3 topics without any time limitation. All the authors contributed equally to this work and to the s-meeting.

Table 1 Fraction of unimodal and bimodal distribution in the ensemble surrogate distribution for the three sectors of the WAI-JSI phase space defined in the text. The bold characters the values obtained from NCEP; in parentheses are the values obtained from ERA40.

Figure 1. Orographic resonance curve allowing for the nonlinear wave self interaction. The observational evidence that the westerlies strength (tropospheric jet) is uniformly distributed, while the activity of the ultra-long planetary waves has a bimodal distribution, imposes to take into account the nonlinearity due to wave self-interaction. The nonlinear term bends the orographic resonant curve of the index of the Wave Activity (WAI), producing different states corresponding to the same value of the Jet Strength Index (JSI). Stable equilibria are indicated by the large dots.

Figure 2. Evidence of the dependence of the planetary wave regimes on the jet strength for the winter-time Northern Hemisphere on the 1958-2002 time frame (NCEP dataset). a) Two-dimensional joint pdf using the index of the planetary waves (WAI) and the index of the tropospheric jet strength (JSI). b) One-dimensional pdf of the planetary waves index (WAI) for low JSI (red), intermediate (blue) and for high JSI (black). Units: WAI [m], JSI [m/s].

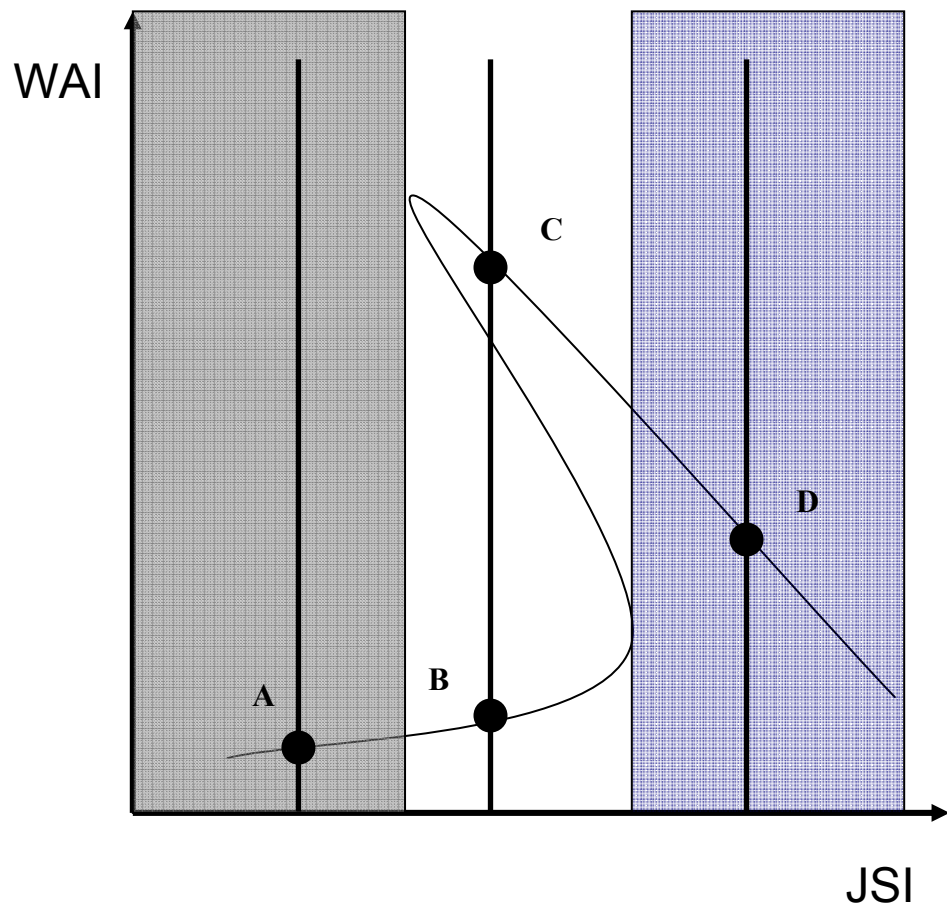
Figure 3. Composites of the spatial patterns corresponding to the peaks of the pdfs shown in Fig 2. Panel i) and ii) show the eddy fields 500 hPa geopotential height pertaining to the pattern A and B, respectively. Panel iii) shows the differences in the 500 hPa geopotential height field between the patterns B and C of the bimodal distribution. Panel iv) shows the eddy fields 500 hPa geopotential

height pertaining to the pattern D. Units are m and contour interval is 50 m for i), ii) and iv), while in panel iii) contour interval is 10 m. Dashed lines pertain to negative values. The corresponding 200hPa zonal wind speed U is reported for each panel in filled contours. Units are m/s and contour interval is 10 m/s.

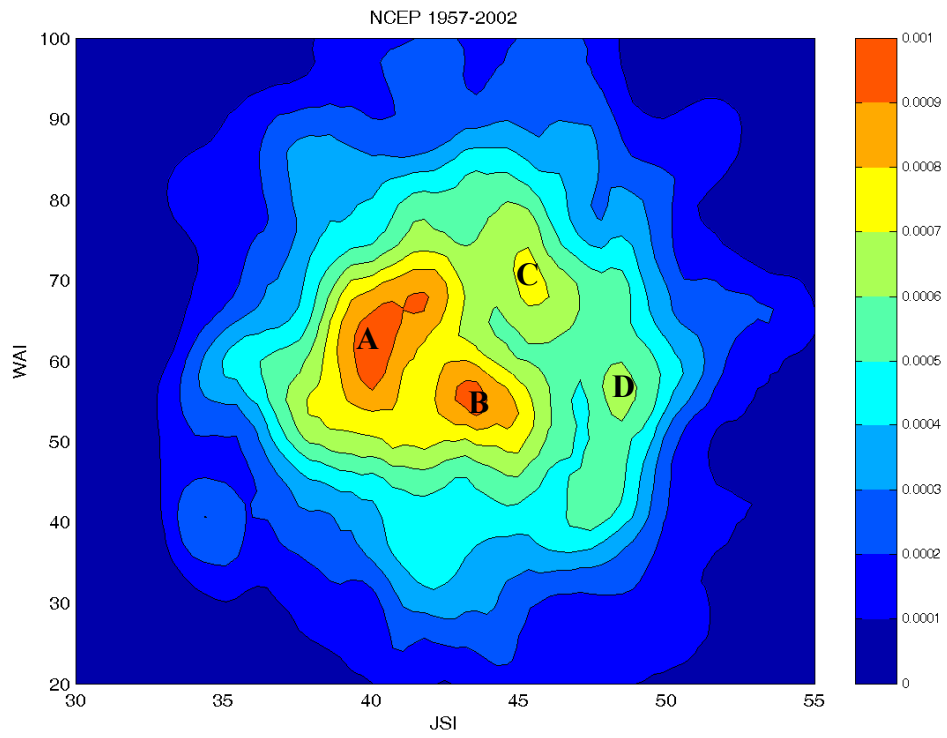
Table 1

	Unimodal	Bimodal
High	0.79 (0.55)	0.07 (0.32)
Intermediate	0.09 (0.16)	0.88 (0.82)
Low	0.94 (0.68)	0.05 (0.29)

Figure 1



a



b

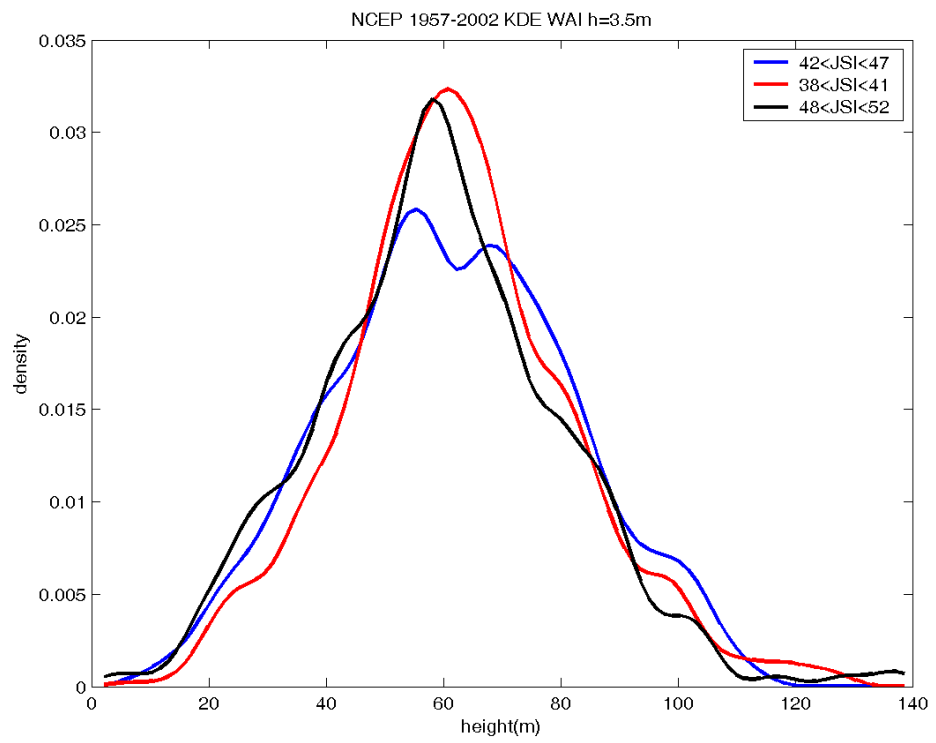


Figure 2

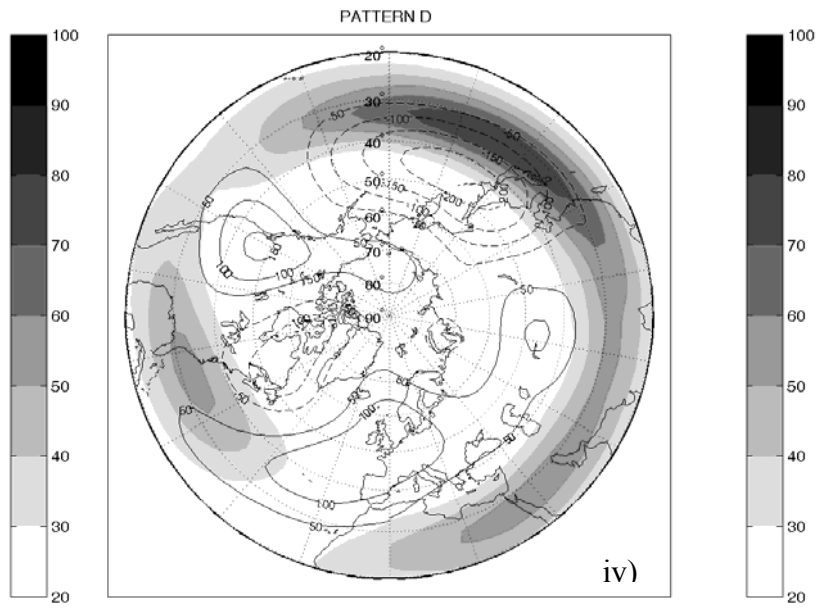
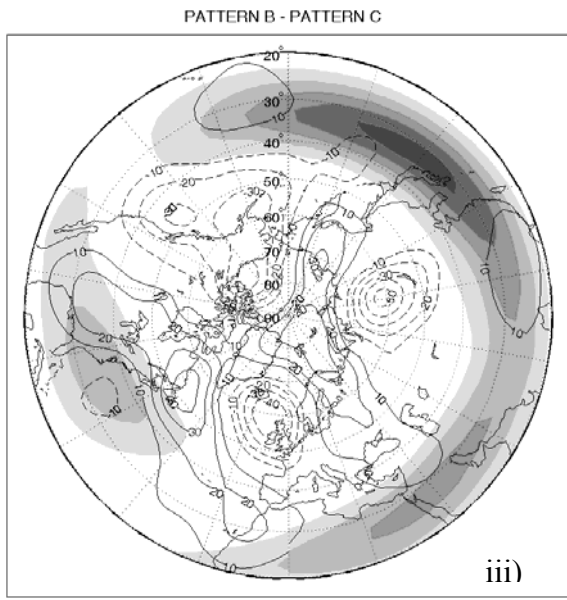
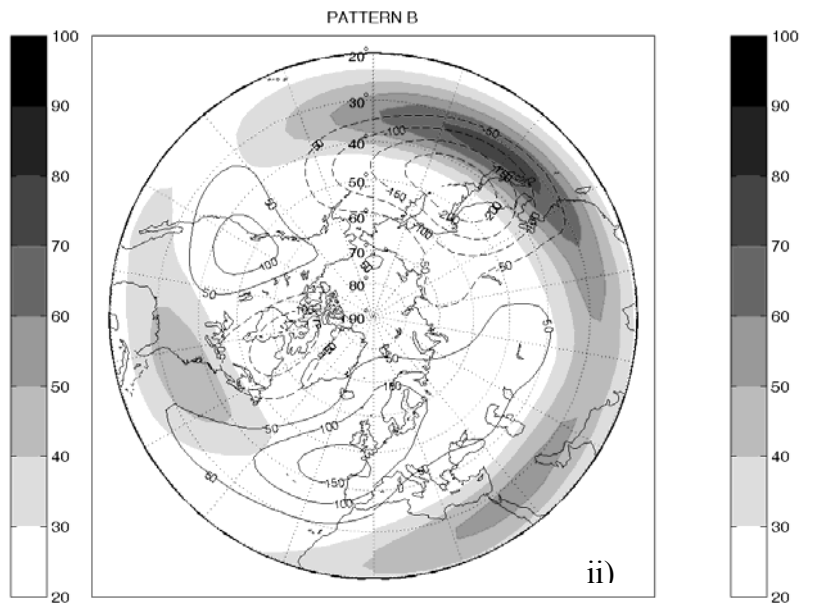
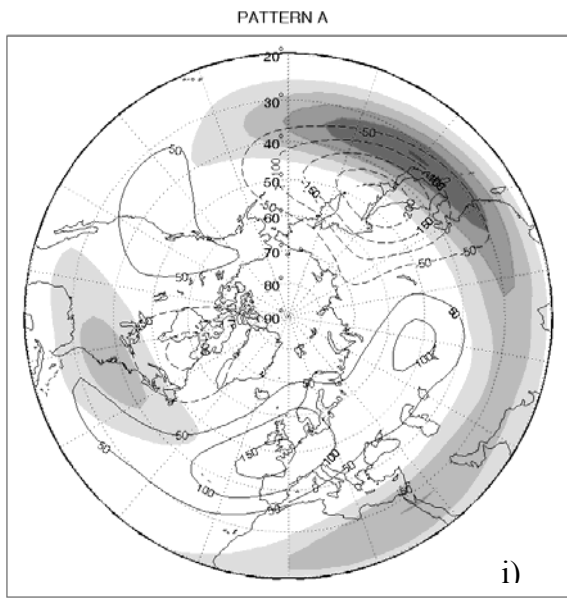


Figure 3